

Pd(0) immobilized on Fe₃O₄@AHBA: an efficient magnetically separable heterogeneous nanocatalyst for C–C coupling reactions

Tonmoy Chakraborty, Abani Sarkar & Tanmay Chattopadhyay

To cite this article: Tonmoy Chakraborty, Abani Sarkar & Tanmay Chattopadhyay (2019): Pd(0) immobilized on Fe₃O₄@AHBA: an efficient magnetically separable heterogeneous nanocatalyst for C–C coupling reactions, Journal of Coordination Chemistry, DOI: [10.1080/00958972.2019.1687890](https://doi.org/10.1080/00958972.2019.1687890)

To link to this article: <https://doi.org/10.1080/00958972.2019.1687890>

 View supplementary material 

 Published online: 11 Nov 2019.

 Submit your article to this journal 

 View related articles 

 View Crossmark data 



Pd(0) immobilized on Fe₃O₄@AHBA: an efficient magnetically separable heterogeneous nanocatalyst for C–C coupling reactions

Tonmoy Chakraborty^a, Abani Sarkar^a and Tanmay Chattopadhyay^b

^aDepartment of Chemistry, University of Calcutta, Kolkata, India; ^bDepartment of Chemistry, Diamond Harbour Women's University, Sarisha, India

ABSTRACT

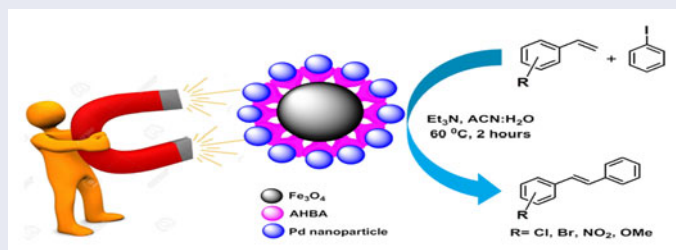
We have developed a new method to synthesize magnetically separable Fe₃O₄@AHBA@Pd(0) (AHBA = 3-amino-4-hydroxybenzoic acid) heterogeneous nanocatalyst via anchoring of palladium(0) on the surface of AHBA-coated Fe₃O₄ nanoparticles. The synthesized nanocatalyst was characterized by FT-IR, PXRD, ICP, XPS, FESEM, EDX, TEM, TGA, BET, and FT-RAMAN analysis. X-ray photoelectron spectroscopy (XPS) indicated the presence of Pd(0) on the surface of Fe₃O₄@AHBA. BET analysis exhibits high surface area of the prepared nanocatalyst with catalytic activity toward Heck coupling reactions with high turnover frequency (TOF) at 60 °C in water–acetonitrile within 2 h. The nanocatalyst can be easily recovered from the reaction mixture by using an external magnet and recycled six times without significant decrease in its catalytic activity. All the isolated products are obtained as solids or oils, fully characterized by ¹H-NMR spectroscopy.

ARTICLE HISTORY

Received 22 May 2019
Accepted 24 September 2019

KEYWORDS

Fe₃O₄@AHBA@Pd(0) nanocatalyst; C–C coupling reaction; magnetically separable; six times reusability



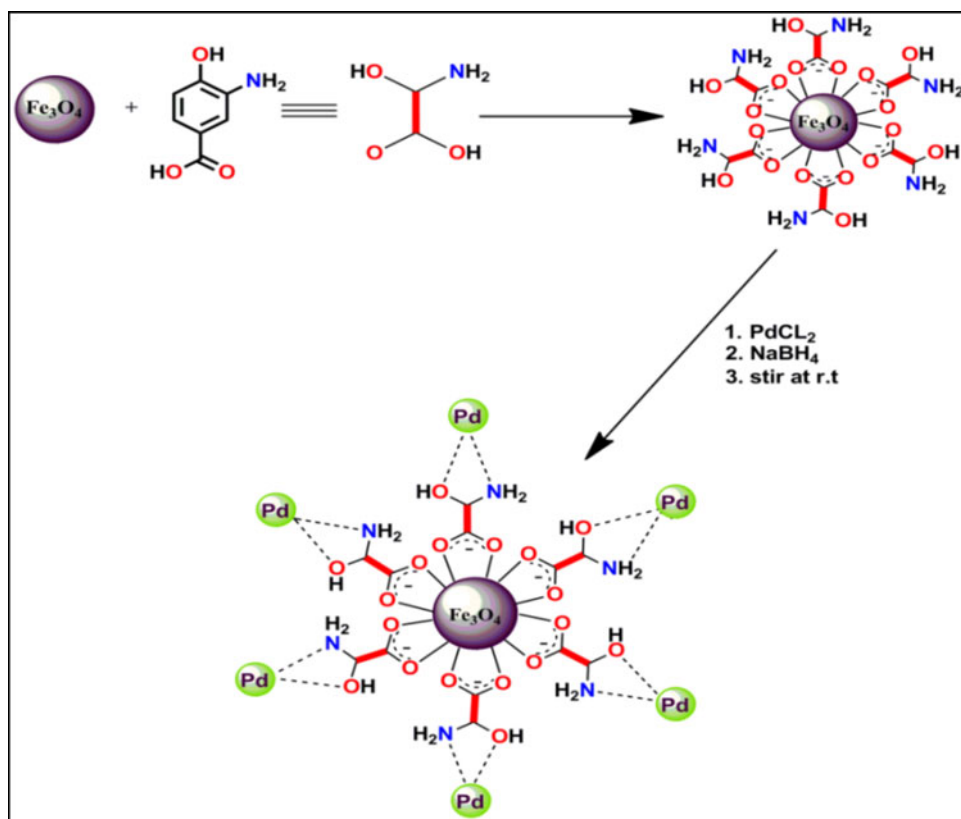
1. Introduction

Palladium compounds are used as homogeneous catalysts [1, 2] in many coupling reactions. Electronegativity [3, 4] of palladium leads to relatively strong Pd–H and Pd–C bonds and also develops a polarized Pd–X bond; it allows easy access of Pd(0) to Pd(II) oxidation states, essential for oxidative addition, transmetalation, and

CONTACT Tanmay Chattopadhyay  tanmayc2003@gmail.com

 Supplemental data for this article can be accessed <https://doi.org/10.1080/00958972.2019.1687890>.

© 2019 Informa UK Limited, trading as Taylor & Francis Group



Scheme 1. Schematic diagram for the preparation of Fe_3O_4 @AHBA@Pd(0).

reductive elimination [5–8]. These homogeneous catalysts have some major drawbacks such as catalyst separation from the reaction mixture, recycling, and product contamination. Heterogenization of metal catalysts can avoid these problems [9–13]. There are two major drawbacks preparing nanoparticles; they tend to aggregate and their recovery is difficult. To prevent aggregation of nanoparticles electrostatic–steric stabilizers like polymers, surfactants and organic ligands are used [14, 15]. Magnetic nanoparticles (MNPs) have been extensively used in immobilization of metal nanoparticles as these catalysts show high activity due to the large surface area and have simple and efficient recycling from the reaction mixtures by applying an external magnetic field, simultaneously with simple decantation of the product from the reaction mixture [16–24]. Although synthesis and applicability of various magnetically separable Pd(0)-nanocatalysts have been reported, including Fe_3O_4 /DAG/Pd [25], Pd/ WO_3 [26], Pd/ Fe_3O_4 @C(MFC) [27], Fe_3O_4 @ SiO_2 -EDTA-Pd NPs [28], Pd@ZPGly [29], Pd/ TiO_2 [30] and Fe_3O_4 @OA-Pd [31] for the Heck reaction. In most cases, the synthetic procedure for nanocatalysts requires complicated steps. Furthermore, the use of toxic organic solvent, high temperature, and long reaction time for catalytic reaction (C–C coupling reactions) are other disadvantages for Pd(0)-nanocatalysts. Therefore, the development of an alternative general and mild procedure employing a stable and inexpensive Pd(0)-nanocatalyst is in demand.

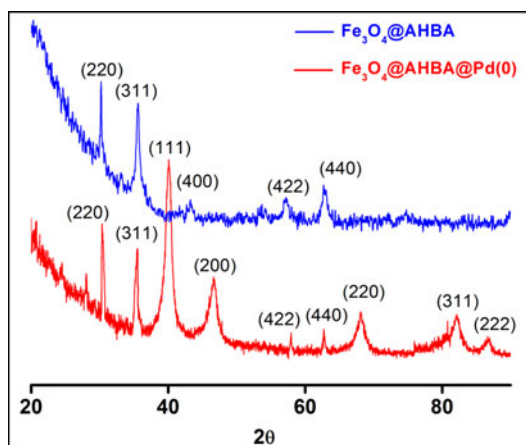


Figure 1. Powder X-ray diffraction spectra of Fe₃O₄@AHBA and Fe₃O₄@AHBA@Pd(0).

Hence, in our present work, we sought to address these challenges by developing a new idea for heterogenizing magnetically separable Pd(0)-nanocatalyst using 3-amino-4-hydroxybenzoic acid (AHBA) decorated iron oxide and palladium nanoparticles for C–C coupling Heck reactions (Scheme 1). Carboxylate of AHBA modified the surface of Fe₃O₄ nanoparticles to form Fe₃O₄@AHBA and that was connected with Pd(0) by formation of a five-membered chelate ring of its free amino and hydroxyl groups enhancing the stability of our synthesized nanocatalyst. The prepared catalyst was characterized by FESEM, HRTEM, EDX, FT-IR, ICP, XPS, FT-RAMAN, DLS, PXRD, and BET analyses. Our synthesized catalyst showed better activity and was environmentally acceptable compared to reported methods. It offered a number of advantages such as simple process, stability of the catalyst, yield in short reaction time using low temperature, easy work-up and separation of the catalyst from the reaction mixture by external magnet, recyclability with minimal loss of activity along with high yield of product.

2. Experimental

2.1. Materials and physical methods

All reagents and chemicals were purchased from Sigma and used without purification. Solvents used for spectroscopic studies were purified and dried by standard procedures before use. FeSO₄·7H₂O, FeCl₃·6H₂O, PdCl₂, and sodium borohydride were purchased from Merck and 3-amino-4-hydroxybenzoic acid and CDCl₃ were purchased from Sigma Aldrich. UV–Vis spectra were recorded on a SHIMADZU UV-2450 spectrophotometer. Infrared spectra (4000–500 cm⁻¹) were recorded at 27 °C using a Perkin-Elmer RXI FT-IR spectrophotometer with KBr pellets. The Pd content of the catalysts was determined by ICP analysis (Varian, Vista-pro). Thermal analyses (TG-DTA) were carried out on a Mettler Toledo (TGA/SDTA851) thermal analyzer in flowing dinitrogen (flow rate: 30 cm³ min⁻¹). Field Emission Scanning Electron Microscope (FESEM) measurement was performed with a JEOL JSM-6700F. Transmission Electron Microscope (TEM) measurement was carried out with a JEOL (Japan) JEM2100 high-resolution transmission electron microscope. X-ray powder diffraction (PXRD) was performed on

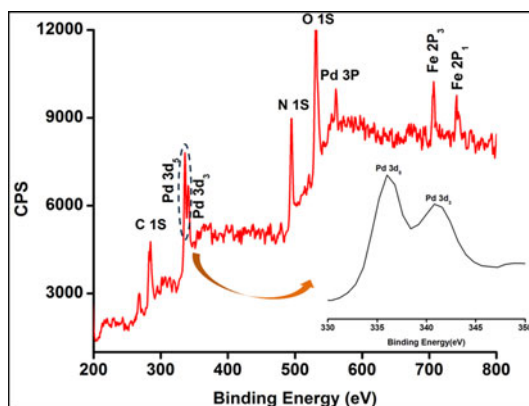


Figure 2. X-ray photoelectron spectroscopy of $\text{Fe}_3\text{O}_4@AHBA@Pd(0)$ taken in full range; inset shows the characteristic band of Pd 3d spectrum.

a XPERT-PRO diffractometer with monochromated $\text{Cu-K}\alpha$ radiation (40.0 kV, 30.0 mA) at room temperature. The irradiation dependent study was done after different irradiation times with a white light source compiled with a <420 nm cut off filter. A vibrating sample magnetometer (EV-9, Microsense and ADE) was utilized for obtaining magnetization curves. $^1\text{H-NMR}$ spectra (300 MHz) were recorded in CDCl_3 on a Bruker AV300 Supercon NMR spectrometer.

2.2. Synthesis of heterogeneous catalysts

2.2.1. Synthesis of Fe_3O_4 NPs

Magnetically separable Fe_3O_4 NPs were synthesized following the reported procedure [32].

2.2.2. Synthesis of $\text{Fe}_3\text{O}_4@AHBA$ (3-amino-4-hydroxybenzoic acid)

3-Amino-4-hydroxybenzoic acid (5 g) was dissolved in 15 mL of ethanol, then ethanolic suspension solution of 5 g of Fe_3O_4 was added to the solution and stirred for 24 h at room temperature. Then the product was allowed to settle and collected using an external magnet, and washed four times with ethanol. The products were air dried.

2.2.3. Synthesis of $\text{Fe}_3\text{O}_4@AHBA@Pd(0)$

$\text{Fe}_3\text{O}_4@AHBA$ (1 g) was dispersed in water (25 mL) by stirring, then PdCl_2 (200 mg) was added slowly to the suspension and the solution was stirred for 24 h at room temperature. The product was collected by centrifugation, washed with water to produce $\text{Fe}_3\text{O}_4@AHBA@PdCl_2$, then 0.2 g of NaBH_4 was added to the solution which was stirred for 24 h at room temperature. The black precipitate of $\text{Fe}_3\text{O}_4@AHBA@Pd(0)$ catalyst was separated using an external magnet and washed with water several times. The product was collected and dried under vacuum at 60°C for 1 h. The Pd content of the catalyst was determined by ICP to be 0.62 mol%.

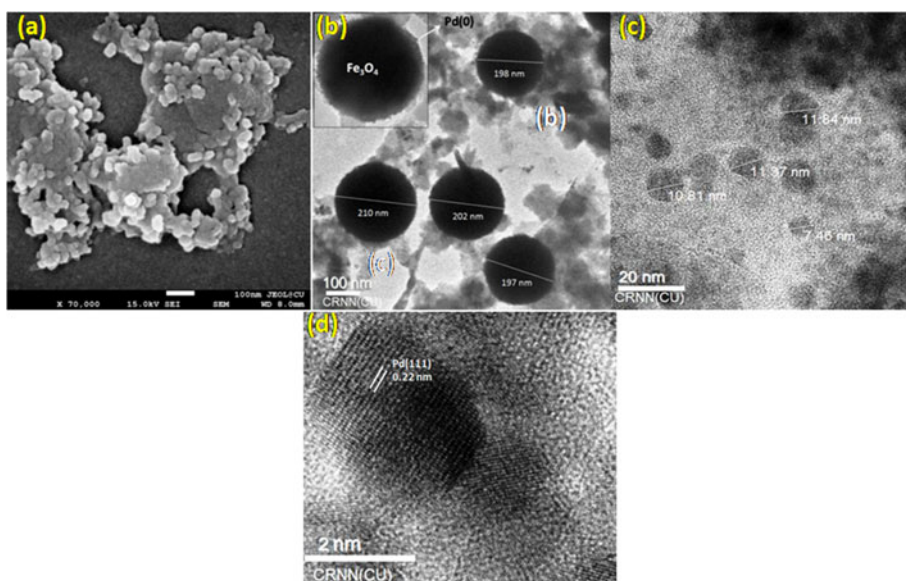


Figure 3. (a) FESEM image; (b) TEM image (zoom out); (c) TEM image (zoom in); and (d) HRTEM with lattice fringe of $\text{Fe}_3\text{O}_4\text{@AHBA@Pd(0)}$.

2.2.4. General procedure of coupling reaction

A mixture of alkene (2.5 mmol), aryl halide (2 mmol), Et_3N (2 mmol), catalyst (20 mg, Pd: 0.62 mol%) in H_2O , and acetonitrile (30 ml) was refluxed at 60°C for 2 h. The catalyst was separated magnetically and the mixture was filtered and concentrated *in vacuo*; the residue was diluted with Et_2O . The organic layer was washed several times with brine, dried over MgSO_4 , filtered, and concentrated *in vacuo* to give the crude product.

3. Results and discussion

3.1. Synthesis and characterization of $\text{Fe}_3\text{O}_4\text{@AHBA@Pd(0)}$

Fe_3O_4 nanoparticles were prepared following the reported procedure. Then $\text{Fe}_3\text{O}_4\text{@AHBA@Pd(0)}$ was prepared by stirring $\text{Fe}_3\text{O}_4\text{@AHBA}$ with PdCl_2 for 24 h in water and finally NaBH_4 was added for reduction of Pd^{+2} to Pd^0 .

Primarily, the reduction of $\text{Fe}_3\text{O}_4\text{@AHBA@PdCl}_2$ to $\text{Fe}_3\text{O}_4\text{@AHBA@Pd(0)}$ was confirmed by UV–Vis spectroscopy in solution (Figure S1, supplementary material). The UV–Vis spectra of PdCl_2 solution showed a peak at 416 nm but after addition of NaBH_4 the reduction of Pd^{+2} to Pd^0 occurred and the peaks disappeared with a constant change in color from yellow to black due to the formation of palladium nanoparticles.

FT-IR spectra of $\text{Fe}_3\text{O}_4\text{@AHBA}$ showed a sharp band at 1600 cm^{-1} which was the $\text{C}=\text{O}$ stretching frequency of carboxylic acid group and another broad band at 3450 cm^{-1} due to free $\text{O}-\text{H}$ and NH_2 groups of AHBA. The bands at 620 and 586 cm^{-1} were due to Fe_3O_4 NPs, the signature $\text{Fe}-\text{O}$ vibration [33]; all these peaks were also present in $\text{Fe}_3\text{O}_4\text{@AHBA@Pd(0)}$ but all the peaks were broadened and underwent a low-frequency shift of wavelength for the stretch. FT-IR spectra of $\text{Fe}_3\text{O}_4\text{@AHBA@Pd(0)}$ and $\text{Fe}_3\text{O}_4\text{@AHBA}$ are shown in Figure S2 (supplementary material).

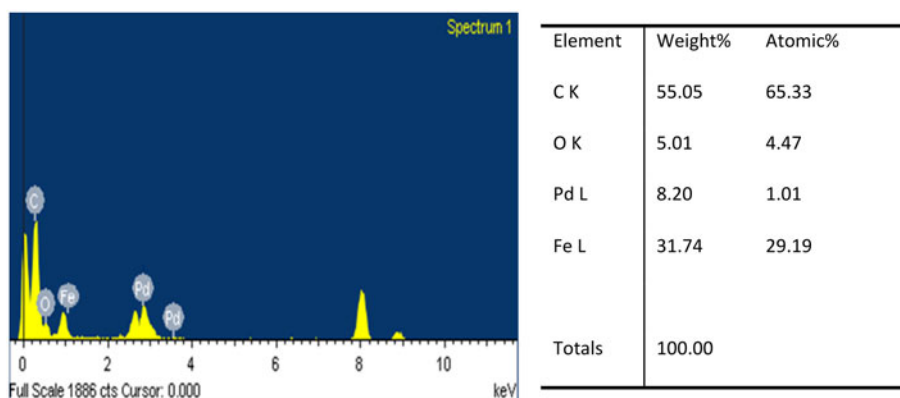


Figure 4. EDX spectrum $\text{Fe}_3\text{O}_4\text{@AHBA@Pd}(0)$ and calculated weight percentage of elements.

TGA analysis of Fe_3O_4 and $\text{Fe}_3\text{O}_4\text{@AHBA@Pd}(0)$ was examined from 40°C to 800°C (Figure S3, supplementary material). TGA curve of $\text{Fe}_3\text{O}_4\text{@AHBA@Pd}(0)$ consists of a weight loss about 18% from 250 to 800°C whereas for Fe_3O_4 nanoparticles it was about 6.5%. The enhanced weight loss is due to increasing amount of attached organic moiety from Fe_3O_4 to $\text{Fe}_3\text{O}_4\text{@AHBA@Pd}(0)$.

The PXRD data of $\text{Fe}_3\text{O}_4\text{@AHBA}$ (Figure 1) showed the diffraction peaks at $2\theta = 29.8^\circ, 35.39^\circ, 42.6^\circ, 56.55^\circ$ and 62.36° which can be assigned to the (220), (311), (400), (422), and (440) planes of Fe_3O_4 [34]. The same peaks are observed in $\text{Fe}_3\text{O}_4\text{@AHBA@Pd}(0)$ with addition of other diffraction peaks at $2\theta = 40^\circ, 46.6^\circ, 68.1^\circ, 82^\circ,$ and 86.8° which can be assigned to the (111), (200), (220), (311), and (222) planes, respectively, for Pd(0) [35]. PXRD patterns indicate that the magnetically separable nanoparticles contain pure Fe_3O_4 with a spinel structure and Pd(0) [36]. That is why the grafting process does not induce any phase change of Fe_3O_4 but only the peak intensity decreases slightly. The size of the synthesized nanoparticles has been calculated using the Debye-Scherrer equation, $D = k\lambda/\beta\cos\theta$ ($k = \text{constant}, 0.94$), where k is the wavelength of Cu-K α (1.54 Å), β is the corrected diffraction line full-width at half-maximum (FWHM), and θ is Bragg's angle. Using this equation, the size of the Pd(0) nanoparticles at $2\theta = 41^\circ$ is calculated to be 10.57 nm.

The chemical state of palladium in $\text{Fe}_3\text{O}_4\text{@AHBA@Pd}(0)$ was assessed by XPS (Figure 2). The binding energies in the XPS spectra are calibrated by using that of C 1s (284 eV); this signal comes mainly due to instrumental treatment before the XPS test. Another major peak at 532 eV is due to O 1s spectrum [37]. Two minor peaks at 710 and 730 eV are due to Fe 2p₃ and Fe 2p₁, respectively [38]. The binding energies in the XPS spectra showed two peaks at 335.5 and 340.8 eV for Pd 3d₅ and Pd 3d₃, attributed to Pd(0) [39]. Figure S4 (supplementary material) showed the XPS spectra of $\text{Fe}_3\text{O}_4\text{@AHBA@Pd}(0)$ and free palladium nanoparticles only.

FESEM images of $\text{Fe}_3\text{O}_4\text{@AHBA@Pd}(0)$ presented in Figure 3a suggest that the Pd(0) NPs have roughly spherical and hexagonal shaped morphology within the range of 15–20 nm size and the average diameter is 16 nm. TEM images of $\text{Fe}_3\text{O}_4\text{@AHBA@Pd}(0)$ (Figure 3(b)) revealed that the diameter of the prepared $\text{Fe}_3\text{O}_4\text{@AHBA}$ nanoparticles was 200 nm and each $\text{Fe}_3\text{O}_4\text{@AHBA}$ surface was uniformly decorated by palladium

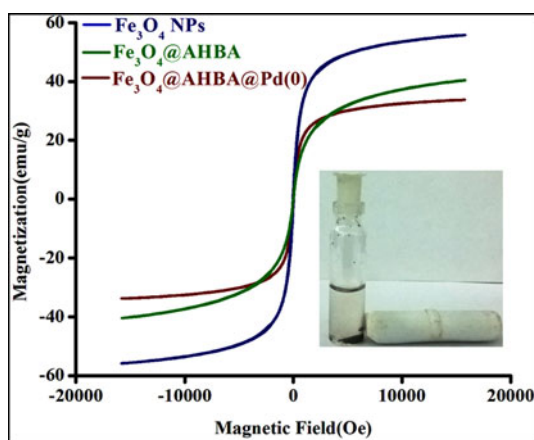


Figure 5. Magnetic curves of Fe_3O_4 , $\text{Fe}_3\text{O}_4@AHBA$ and $\text{Fe}_3\text{O}_4@AHBA@Pd(0)$; inset shows the picture of magnetic separation.

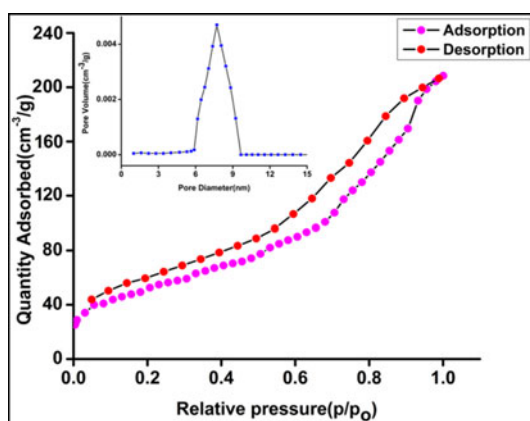


Figure 6. Adsorption-desorption isotherm of $\text{Fe}_3\text{O}_4@AHBA@Pd(0)$; inset shows pore size distribution of $\text{Fe}_3\text{O}_4@AHBA@Pd(0)$.

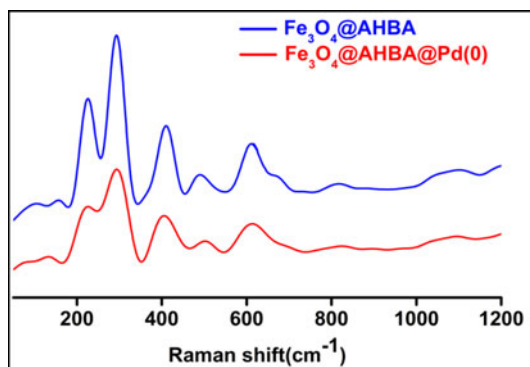
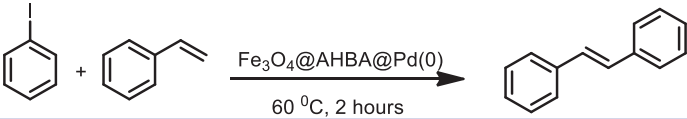


Figure 7. FT-RAMAN spectrum of $\text{Fe}_3\text{O}_4@AHBA$ and $\text{Fe}_3\text{O}_4@AHBA@Pd(0)$.

nanoparticles. **Figure 3c** shows the higher magnification TEM image of $\text{Fe}_3\text{O}_4@AHBA@Pd(0)$. The spherical morphology of Pd(0) NPs on the surface of

Table 1. Optimization of $\text{Fe}_3\text{O}_4\text{@AHBA@Pd(0)}$ for Heck coupling between iodobenzene and styrene.


| Entry | Base | Solvent | Time (h) | Yield (%) ^a |
|-------|--|--|----------|------------------------|
| 1 | K_2CO_3 | $\text{H}_2\text{O}/\text{Acetonitrile}^b$ | 6 | 68 |
| 2 | Na_2CO_3 | $\text{H}_2\text{O}/\text{Acetonitrile}^b$ | 6 | 59 |
| 3 | NaHCO_3 | $\text{H}_2\text{O}/\text{Acetonitrile}^b$ | 6 | 66 |
| 4 | NaOAc | $\text{H}_2\text{O}/\text{Acetonitrile}^b$ | 6 | 69 |
| 5 | Cs_2CO_3 | $\text{H}_2\text{O}/\text{Acetonitrile}^b$ | 6 | 52 |
| 6 | No base | $\text{H}_2\text{O}/\text{Acetonitrile}^b$ | 14 | 0 |
| 7 | Et_3N | $\text{H}_2\text{O}/\text{Acetonitrile}^b$ | 2 | 97 |
| 8 | Et_3N (no catalyst) | $\text{H}_2\text{O}/\text{Acetonitrile}^b$ | 14 | 0 |
| 9 | Et_3N (using Fe_3O_4) | $\text{H}_2\text{O}/\text{Acetonitrile}^b$ | 14 | 0 |
| 10 | Et_3N (using $\text{Fe}_3\text{O}_4\text{@AHBA}$) | $\text{H}_2\text{O}/\text{Acetonitrile}^b$ | 14 | 0 |

^aReaction conditions: iodobenzene (2 mmol), styrene (2.5 mmol), base (2 mmol), 20 mg, 0.60 mol% catalyst ($\text{Fe}_3\text{O}_4\text{@AHBA@Pd(0)}$).

^b1:1.

$\text{Fe}_3\text{O}_4\text{@AHBA}$ have diameters within the range of 7–12 nm and average diameter of 11 nm. The size of the Pd(0) nanoparticles calculated from PXRD corroborates well with the size, obtained from TEM images. Figure 3d shows the lattice fringes of the palladium nanoparticles as well as the electron diffraction pattern; the interplanar spacing was about 0.220 nm, corresponding to the orientation of “111” atomic planes of palladium nanoparticles.

Energy-dispersive X-ray (EDX) spectrum of $\text{Fe}_3\text{O}_4\text{@AHBA@Pd(0)}$ is depicted in Figure 4. Here the signals for Fe and Pd are due to the presence of Fe_3O_4 and palladium nanoparticles, respectively.

The hydrodynamic size of $\text{Fe}_3\text{O}_4\text{@AHBA@Pd(0)}$ was represented by dynamic light scattering (DLS), Figure S6 (supplementary material). The calculated mean diameter was 220–230 nm measuring the entire particle (Fe_3O_4 and Pd combined). For TEM measurements the size estimated was for dried catalyst, whereas DLS measures the size in the hydrated state of the sample, so the size measured by DLS is a hydrodynamic diameter and is comparatively larger than that calculated from TEM.

Figure 5 shows the magnetization behavior of (a) Fe_3O_4 NPs, (b) $\text{Fe}_3\text{O}_4\text{@AHBA}$, and (c) $\text{Fe}_3\text{O}_4\text{@AHBA@Pd(0)}$ under applied magnetic field. The curves reveal similar phenomena as observed earlier [36, 40]. The decrease in the values of the saturation magnetization (M_s) from the Fe_3O_4 nanoparticles (55.90 emu g^{-1}) to $\text{Fe}_3\text{O}_4\text{@AHBA@Pd(0)}$ (40.01 emu g^{-1}) are due to increasing diamagnetic organic moiety from Fe_3O_4 NPs to $\text{Fe}_3\text{O}_4\text{@AHBA@Pd(0)}$. However, the net magnetism of final nanocatalyst $\text{Fe}_3\text{O}_4\text{@AHBA@Pd(0)}$ is good for an effective separation from the solution by external magnetic force.

Figure 6 shows adsorption–desorption isotherm with pore size distribution plot of $\text{Fe}_3\text{O}_4\text{@AHBA@Pd(0)}$ investigated by the Brunauer–Emmett–Teller (BET) gas-sorption measurements carried out at 77 K for the dried powder sample under vacuum. From the BET analysis, the main pore size of the catalyst was 7.9 nm and surface area was $230 \text{ m}^2\text{g}^{-1}$. Due to the high surface area of our synthesized nanocatalyst, it provided a great platform for coupling reactions.

Table 2. Optimization of catalyst concentration $\text{Fe}_3\text{O}_4\text{@AHBA@Pd(0)}$ for the reaction of Heck coupling between iodobenzene and styrene.

| Entry | Catalyst (mol% Pd) | Solvent | Yield (%) ^a |
|-------|--------------------|-----------------------|------------------------|
| 1 | 0.700 | H ₂ O/ACN | 78 |
| 2 | 0.500 | H ₂ O/ACN | 82 |
| 3 | 0.400 | H ₂ O/ACN | 77 |
| 4 | 0.600 | H ₂ O/ACN | 92 |
| 5 | 0.300 | H ₂ O/ACN | 70 |
| 6 | 0.500 | H ₂ O/EtOH | 80 |
| 7 | 0.600 | H ₂ O/EtOH | 86 |
| 8 | 0.600 | H ₂ O/DMF | 68 |
| 9 | 0.600 | DMF | 55 |
| 10 | 0.600 | H ₂ O/MeOH | 82 |

^aReaction conditions: iodobenzene (2 mmol), styrene (2.5 mmol), base Et₃N (2 mmol), time (2 h).

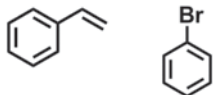
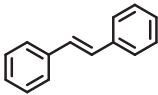
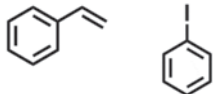
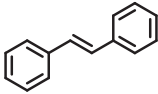
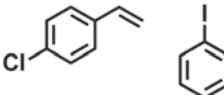
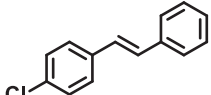
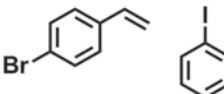
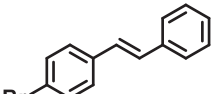
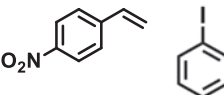
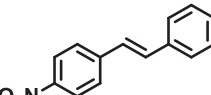
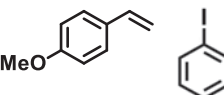
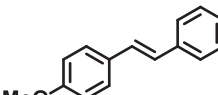
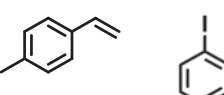
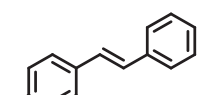
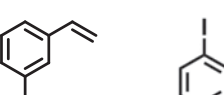
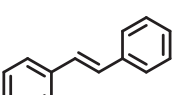
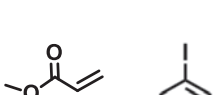
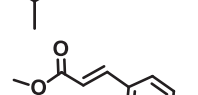
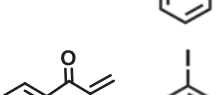
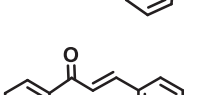
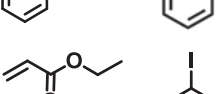
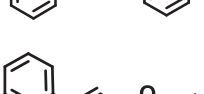
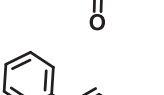
FT-Raman spectra were recorded using a LabRAM HR spectrometer equipped with an air-cooled argon ion (Ar^+) laser of wavelength 488 nm and a Peltier-cooled charge-coupled-device (CCD) detector, measured between 100–1200 cm^{-1} at room temperature (Figure 7) for $\text{Fe}_3\text{O}_4\text{@AHBA}$ and $\text{Fe}_3\text{O}_4\text{@AHBA@Pd(0)}$, respectively. The Raman spectrum of $\text{Fe}_3\text{O}_4\text{@AHBA}$ showed peaks at 222 (weak), 290 (strong), 405 (weak), 487 (weak), and 613 (weak) cm^{-1} ; these values were slightly shifted from Fe_3O_4 [41] after coating with AHBA. Also the spectra of $\text{Fe}_3\text{O}_4\text{@AHBA}$ and $\text{Fe}_3\text{O}_4\text{@AHBA@Pd(0)}$ are similar to each other. Thus the surface of catalyst contains palladium as a zero oxidation state (without any PdO) which was further confirmed by XPS study.

To optimize the reaction conditions, a series of experiments were performed using styrene (2.5 mmol) and iodobenzene (2 mmol) with $\text{Fe}_3\text{O}_4\text{@AHBA@Pd(0)}$ under various reaction conditions (Table 1). The effect of the concentration of the catalyst was studied (Table 2) using different solvent/mixtures. In absence of catalyst the conversion was low (Table 1, entry 8). The maximum conversion is observed when the reaction was performed in the presence of 20 mg, 0.60 mol% of catalyst; Et₃N (2 mmol) and catalyst (20 mg, 0.60 mol%) in H₂O/acetonitrile (30 ml) was ideal for coupling of styrene with iodobenzene. After 2 h the conversion of reaction remains constant, the reaction catalyst was separated magnetically and the mixture was filtered and concentrated *in vacuo*. The residue was diluted with Et₂O. The organic layer was washed several times with brine, dried over MgSO₄, filtered, and concentrated *in vacuo* to give the crude product. In the absence of base or catalyst the reaction failed to produce any product and we also performed in the presence of only Fe_3O_4 and $\text{Fe}_3\text{O}_4\text{@AHBA}$, also without product (Table 1).

To demonstrate the general reactivity of $\text{Fe}_3\text{O}_4\text{@AHBA@Pd(0)}$, a series of substrates were taken using triethylamine as base and water/acetonitrile as solvent (Table 3). The major drawback related with magnetically separable Pd(0) catalysts when water is the reaction solvent is the poor interaction of active Pd with organic substrates. To overcome this drawback, a mixture of organic solvents and water is used as the reaction medium for magnetically separable Pd catalyzed Heck coupling reaction. All reactions proceeded smoothly with very good yield.

Electron withdrawing and donating substituent of styrene showed a significant effect on the substrate reactivity (Table 3) and the reaction with aryl bromide and iodide are equally efficient for coupling. Reactions with aryl chlorides were slow, affording the desired product in only 30% yield. Table 3 (entries 1–12) display the experimental results. In all the coupling reactions transformation of reactant to product occurred

Table 3. Fe₃O₄@AHBA@Pd(0) Catalyzed Heck coupling reactions with various substrates.

| Entry | Substrate | Product | Time (h) | Conversion (%) | Yield ^{a,b} (%) | TOF ^c (h ⁻¹) |
|-------|---|---|----------|----------------|--------------------------|-------------------------------------|
| 1 |  |  | 2 | 97 | 94 | 7.58 |
| 2 |  |  | 2 | 98 | 97 | 7.75 |
| 3 |  |  | 2 | 98 | 95 | 7.66 |
| 4 |  |  | 2 | 97 | 95 | 7.66 |
| 5 |  |  | 2 | 98 | 86 | 6.94 |
| 6 |  |  | 2 | 98 | 93 | 7.50 |
| 7 |  |  | 2 | 97 | 95 | 7.66 |
| 8 |  |  | 2 | 97 | 94 | 7.58 |
| 9 |  |  | 2 | 98 | 92 | 7.42 |
| 10 |  |  | 2 | 96 | 85 | 6.85 |
| 11 |  |  | 2 | 97 | 92 | 7.40 |
| 12 |  |  | 2 | 93 | 90 | 7.26 |

^aReaction conditions: alkene (2.5 mmol), aryl halide (2 mmol), Et₃N (2 mmol), catalyst (20 mg, 0.62 mol%) in 1:1 H₂O–acetonitrile (30 ml), time (2 h).

^bIsolated yield.

^cTOF was defined as mol_{product} mol⁻¹_{Pd} h⁻¹.

Table 4. Catalytic performance of different magnetically separable Pd-based nanocatalysts in coupling of iodobenzene and styrene.

| Entry | Catalyst | Pd (mol%) | Solvent | Base | Temp (°C) | Time (h) | Yield (%) | Ref. |
|-------|---|-----------|----------------------|--------------------------------|-----------|----------|-----------|-----------|
| 1 | Pd/Fe ₃ O ₄ @Polypyrrole | | DMA | TBA | 120 | 3 | 97 | [51] |
| 2 | Pd/N-MCNPs | 1.2 | DMAN | Et ₃ N | 120 | 3 | 97.6 | [52] |
| 3 | Pd-biomagnetite | 5 | DMF | Et ₃ N | 120 | 3 | 100 | [53] |
| 4 | Fe ₃ O ₄ -NH ₂ -Pd | 8.83 | NMP | K ₂ CO ₃ | 130 | 10 | >99 | [54] |
| 5 | Pd/NiFe ₂ O ₄ | 8.54 | DMF | TEA | 80 | 4 | 97 | [55] |
| 6 | Pd/MFC | 0.308 | DMF | K ₂ CO ₃ | 120 | 4 | 100 | [27] |
| 7 | Fe ₃ O ₄ /DAG/Pd | 0.280 | DMF | Et ₃ N | 110 | 3 | 98 | [25] |
| 8 | Fe ₃ O ₄ @AHBA@Pd(0) | 0.60 | H ₂ O/ACN | Et ₃ N | 60 | 2 | 96 | This work |

DMA: N,N-dimethylacetamide; TBA: tributylamine; Pd/N-MCNPs: Pd/N-dopand magnetic carbon nanoparticles; DMAN: dimethylacrylonitrile; Et₃N: triethylamine; NMP: N-methyl-2-pyrrolidone.

with >90% conversion and >85% yield. The ¹H-NMR spectra of the isolated products are given in the Supporting Information.

We compared the results achieved in the present manuscript with reported magnetically separable Pd-based nanocatalysts. In previous work magnetically separable Pd nanocatalysts such as MgFe₂O₄@SiO₂-PrNH₂/Pd/BMO [42], NiFe₂O₄@TABMA-Pd(0) [43], Pd@Hal-2N-TCT-EDA [44], Fe₃O₄@dopa@ML [45], Pd-NHC [46], Fe₃O₄-supported Schiff-base complexes [47], alumina-supported Pd catalysts [48], PdCl₂(NHC)(PPh₃) [49], and PEPPSI-type palladium NHC complex [50] were prepared for various coupling reactions by different techniques and using different functionalizing agents like SiO₂-PrNH₂, TABMA, Hal-2N-TCT-EDA, alumina, dopa, NHC (N-heterocyclic carbene complexes) and Schiff base complexes. The functionalizing agent was used to enhance the stability of nanocatalyst. Most of the catalysts required high temperature, several steps and cost effective reagents during the preparation of catalyst. Here we prepared very cheap and economical friendly magnetically separable Pd nanocatalysts using AHBA (3-amino-4-hydroxybenzoic acid) as a functionalizing agent. Carboxylate of AHBA modified the surface of Fe₃O₄ nanoparticles to form Fe₃O₄@AHBA and that was connected with Pd(0) by formation of five-membered chelate rings of its free amino and hydroxyl group. Then the prepared catalyst was used for C–C (Heck) coupling reactions. For iodobenzene reacting with styrene as a model substrate, the results are listed in Table 4. The results in this work has advantages: low temperature in short reaction time with high turnover frequency (TOF) and the solvent (H₂O/acetonitrile) used here is much preferred to DMA, TBA and DMAN used elsewhere.

The recyclability of Fe₃O₄@AHBA@Pd(0) was examined by removing it from the reaction media by magnet (external magnetic field), the catalyst was washed with water-ethanol (50% v/v) solution and regenerated catalyst was reused under the optimum reaction conditions. The regenerated catalyst was further characterized by PXRD, FESEM, and TEM (Figure 8); after the sixth cycle the catalyst size, shape and morphology were the same. No significant changes were observed in the composition of the regenerated catalyst. Also ICP analysis indicated leaching of 2.2% of palladium after the sixth cycles, which suggests the heterogeneous nature of the nanocatalyst. Reasonable yields of products of the coupling reaction were observed for the sixth reaction cycle as evident from Figure 9.

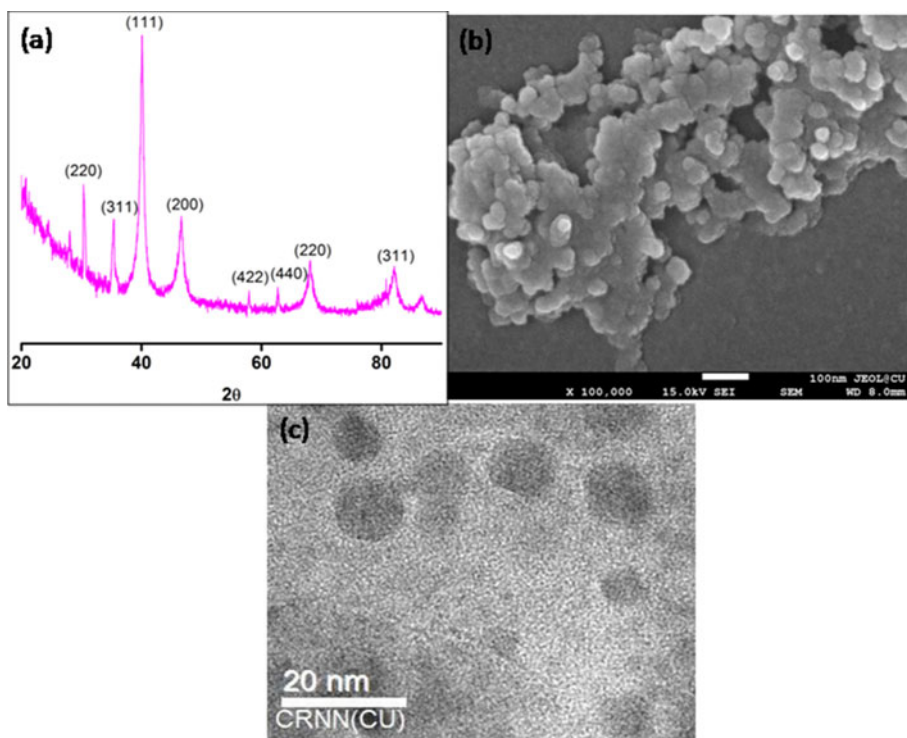


Figure 8. (a) PXRD pattern; (b) FESEM image; (c) TEM image of reused catalyst of $\text{Fe}_3\text{O}_4\text{@AHBA@Pd(0)}$ toward coupling reaction.

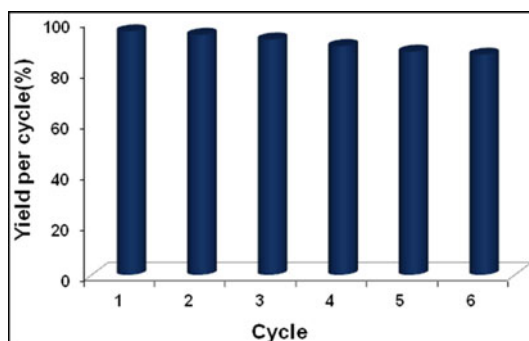


Figure 9. Catalytic activity of $\text{Fe}_3\text{O}_4\text{@AHBA@Pd(0)}$ as a function of reusability of the catalyst.

4. Conclusion

We have synthesized a simple, economical, environmentally friendly, efficient and sustainable magnetically separable $\text{Fe}_3\text{O}_4\text{@AHBA@Pd(0)}$ heterogeneous catalyst for coupling reaction of aryl halides and styrene in the presence of triethylamine as a base at 60°C for 2 h. Our synthesized catalyst showed excellent catalytic properties toward coupling (yield $>85\%$) reactions. Our catalyst has advantages compared to other reported catalysts, such as simple process, stability of the catalyst, use of magnetic nanoparticles as support, effortless recovery, yield in short reaction time using low

temperature with high turnover frequency (TOF), easy work-up and separation of the catalyst from the reaction mixture by external magnet, recyclability for at least six times with minimal loss of activity along with high yield of product. Thus this magnetically separable heterogeneous catalyst could find utilization in several important catalytic processes as well as the common synthetic organic transformations.

Acknowledgements

T. C. is thankful to the UGC-JRF for providing a fellowship [Ref. No: 21/06/2015(i) EU-V]. A. S. is thankful to the CSIR-JRF for providing a fellowship [sanction number 09/028(1005)/2017-EMR-1]. The authors wish to thank the University of Calcutta for providing the facility of the FESEM, HRTEM, PXRD, and FT-IR by the DST FIST program.

Disclosure statement

No potential conflict of interest was reported by the authors.

Funding

Financial support by the Department of Higher Education, Science & Technology and Biotechnology, Government of West Bengal [Memo No. 21(Sanc.)/ST/P/S&T/15G-16/2017 dt. 12-06-2018] is gratefully acknowledged by T. C.

References

- [1] R.H. Crabtree. *Science*, **295**, 288 (2002).
- [2] G. Audi, O. Bersillon, J. Blachot, A.H. Wapstra. *Nucl. Phys. A*, **729**, 3(2003).
- [3] H.R. Crabtree. *John Wiley and Sons*, **392**, (2009).
- [4] C.E. Garrett, K. Prasad. *Adv. Synth. Catal.*, **346**, 889 (2004).
- [5] F. Martin. *Tenth International Conference on Cold Fusion*. Cambridge, MA: World Scientific Publishing, 8, 978 and 256 (2003).
- [6] A.F. Littke, G.C. Fu. *Angew. Chem. Int. Ed.*, **41**, 4176 (2002).
- [7] O. Navarro, R.A. Kelly, S.P. Nolan. *J. Am. Chem. Soc.*, **125**, 16194 (2003).
- [8] L. Botella, C. Najera. *Angew. Chem. Int. Ed.*, **41**, 179 (2002).
- [9] N. Mizuno, M. Misono. *Chem. Rev.*, **98**, 199 (1998).
- [10] F. Lefebvre, J.M. Basset. *J. Mol. Catal. A: Chem.*, **146**, 3 (1999).
- [11] J.M. Thomas. *Angew. Chem. Int. Ed.*, **38**, 3588 (1999).
- [12] M. Pillinger, I.S. Gonçalves, A.D. Lopes, J. Madureira, P. Ferreira, A.A. Valente, T.M. Santos, J. Rocha, J.F.S. Menezes, L.D. Carlos. *J. Chem. Soc., Dalton Trans.*, 1628 (2001).
- [13] J. Adhikary, A. Guha, T. Chattopadhyay, D. Das. *Inorg. Chim. Acta*, **406**, 1 (2013).
- [14] D. Astruc, F. Lu, J.R. Aranzas. *Angew. Chem. Int. Ed.*, **44**, 7852 (2005).
- [15] S. Nath, S. Jana, M. Pradhan, T. Pal. *J. Colloid Interf. Sci.*, **341**, 333 (2010).
- [16] (a) P.D. Stevens, G. Li, J. Fan, M. Yen, Y. Gao. *Chem. Commun.*, **0**, 4435 (2005).(b) S. Wittmann, A. Schatz, R.N. Grass, W.J. Stark, O. Reiser. *Angew. Chem. Int. Ed.*, **49**, 1867 (2010).
- [17] R.B. Nasir Baig, R.S. Varma. *Chem. Commun.*, **48**, 2582 (2012).
- [18] A.-H. Lu, W. Schmidt, N. Matoussevitch, H. Bönemann, B. Spliethoff, B. Tesche, E. Bill, W. Kiefer, F. Schüth. *Angew. Chem. Int. Ed.*, **43**, 4303 (2004).
- [19] R.L. Oliveira, P.K. Kiyohara, L.M. Rossi. *Green Chem.*, **12**, 144 (2010).
- [20] T. Zeng, L. Yang, R. Hudson, G. Song, A.R. Moores, C.J. Li. *Org. Lett.*, **13**, 442 (2011).

- [21] R.S. Varma. *Sustain. Chem. Process*, **2**, 11 (2014).
- [22] M.B. Gawande, A.K. Rathi, P.S. Branco, R.S. Varma. *Appl. Sci.*, **3**, 656 (2013).
- [23] M.B. Gawande, P.S. Branco, R.S. Varma. *Chem. Soc. Rev.*, **42**, 3371 (2013).
- [24] R.B.N. Baig, R.S. Varma. *Green Chem.*, **15**, 398 (2013).
- [25] H. Veisi, A. Sedrpoushan, S. Hemmati. *Appl. Organometal. Chem.*, **29**, 825 (2015).
- [26] M. Amini, D.B. Heydarloo, M. Rahimi, M.G. Kim, S. Gautam, K.H. Chae. *Mater. Res. Bull.*, **83**, 179 (2016).
- [27] M. Zhu, G. Diao. *J. Phys. Chem. C*, **115**, 24743 (2011).
- [28] M. Esmaeilpour, S. Zahmatkesh, N. Fahimi, M. Nosratabadi. *Appl. Organomet. Chem.*, **32**, 4302 (2018).
- [29] V. Kozell, T. Giannoni, M. Nocchetti, R. Vivani, O. Piermatti, L. Vaccaro. *Catalysts*, **7**, 186 (2017).
- [30] L.O. Nyangasi, D.M. Andala, C.O. Onindo, J.C. Ngila, B.C.E. Makhubela, E.M. Ngigi. *J. Nanomater.*, **13** (2017).
- [31] E. Rafiee, A. Ataei, M. Joshaghani. *LOC*, **11**, 707 (2014).
- [32] V. Polshettiwar, B. Baruwati, R.S. Varma. *Green Chem.*, **11**, 127 (2009).
- [33] R.K. Sharma, Y. Monga, A. Puri. *J. Mol. Catal. A: Chem.*, **393**, 84 (2014).
- [34] H. Wan, Z. Wu, W. Chen, G. Guan, Y. Cai, C. Chen, Z. Li, X. Liu. *J. Mol. Catal. A: Chem.*, **398**, 127 (2015).
- [35] S. Navaladian, B. Viswanathan, T.K. Varadarajan, R.P. Viswanath. *Nanoscale Res. Lett.*, **4**, 181 (2009).
- [36] J. Adhikary, A. Datta, S. Dasgupta, A. Chakraborty, M.I. Menéndez, T. Chattopadhyay. *RSC Adv.*, **5**, 92634 (2015).
- [37] T. Chakraborty, A. Chakraborty, S. Maity, D. Das, T. Chattopadhyay. *Mol. Catal.*, **462**, 104 (2019).
- [38] H. Lee, S.H. Park, S.J. Kim, Y.K. Park, K.H. An, B.J. Kim, S.C. Jung. *J. Nanomater.*, **6**, (2014).
- [39] S. Yang, J. Dong, Z. Yao, C. Shen, X. Shi, Y. Tian, S. Lin, X. Zhang. *Sci. Rep.*, **4**, 4501 (2014).
- [40] S. Dasgupta, A. Chakraborty, S. Chatterjee, T. Chattopadhyay. *Inorg. Chim. Acta*, **474**, 1 (2018).
- [41] P.C. Panta, C.P. Bergmann. *J. Mater. Sci. Eng.*, **5**, 1 (2015).
- [42] M. Mahmoudzadeh, E. Mehdi pour, R. Eisavi. *J. Coord. Chem.*, **72**, 841 (2019).
- [43] H. Naeimi, F. Kiani. *J. Coord. Chem.*, **71**, 1157 (2018).
- [44] S. Sadjadi, M.M. Heravi, B. Masoumi, S.S. Kazemi. *J. Coord. Chem.*, **72**, 119 (2019).
- [45] S. Dasgupta, S. Chatterjee, T. Chattopadhyay. *J. Coord. Chem.*, **72**, 550 (2019).
- [46] L. Boubakri, K. Dridi, A.S. Al-Ayed, I. Ozdemir, S. Yasar, N. Hamdi. *J. Coord. Chem.*, **72**, 516 (2019).
- [47] G. Rezaie, A. Naghipour, A. Fakhri. *J. Coord. Chem.*, **71**, 2924 (2018).
- [48] N. Meyer, Y.D. Coster, M. Devillers, S. Hermans. *J. Coord. Chem.*, **71**, 2304 (2018).
- [49] L. Boubakri, L. Mansour, A.H. Harrath, I. Ozdemir, S. Yaşar, N. Hamdi. *J. Coord. Chem.*, **71**, 183 (2018).
- [50] N. Kaloğlu, İ. Özdemir. *Tetrahedron*, **75**, 2306 (2019).
- [51] S. Ko, J. Jang. *Angew. Chem. Int. Ed.*, **45**, 7564 (2006).
- [52] H. Yoon, S. Ko, J. Jang. *Chem. Commun.*, 1468 (2007).
- [53] V.S. Coker, J.A. Bennett, N.D. Telling, T. Henkel, J.M. Charnock, G.V.D. Laan, R.A.D. Patrick, C.I. Pearce, R.S. Cutting, I.J. Shannon, J. Wood, E. Arenholz, I.C. Lyon, J.R. Lloyd. *ACS Nano*, **4**, 2577 (2010).
- [54] F. Zhang, J. Jin, X. Zhong, S. Li, J. Niu, R. Li, J. Ma. *Green Chem.*, **13**, 1238 (2011).
- [55] Z. Gao, Y. Feng, F. Cui, Z. Hua, J. Zhou, Y. Zhu, J. Shi. *J. Mol. Catal. A: Chem.*, **336**, 51 (2011).